SUPPORTING INFO

Black Phosphorus/Palladium Nanohybrid: Unraveling the Nature of P-Pd Interaction and Application in Selective Hydrogenation

Matteo Vanni,[a,h] Manuel Serrano-Ruiz,[a] Francesca Telesio,[b] Stefan Heun,[b] Martina Banchelli,[c] Paolo Matteini,[c] Antonio Massimiliano Mio,[d] Giuseppe Nicotra,[d] Corrado Spinella,[d] Stefano Caporali,[e] Andrea Giaccherini,[f] Francesco D'Acapito,[g] Maria Caporali,*[a] Maurizio Peruzzini*[a]

[a]CNR-Isituto di Chimica dei Composti Organometallici, Via Madonna del Piano10, 50019 Sesto Fiorentino, Italy

[b]NEST Istituto Nanoscienze-CNR and Scuola Normale Superiore, Piazza S. Silvestro 12, 56127 Pisa, Italy

[c]CNR-IFAC, Via Madonna del Piano10, 50019 Sesto Fiorentino, Italy

[d]CNR-IMM Istituto per la Microelettronica e Microsistemi, VIII strada 5, I-95121 Catania, Italy

[e]Department of Industrial Engineering, University of Florence, Via di S. Marta 3, Florence, 50139, Italy

[f]Department of Earth Sciences, University of Florence, Via La Pira 4, Firenze, 50121, Italy

[g]CNR-IOM-OGG, c/o European Synchrotron Radiation Facility - LISA CRG, Grenoble, France

[h]Department of Biotechnology, Chemistry and Pharmacy, University of Siena, 53100 Siena, Italy

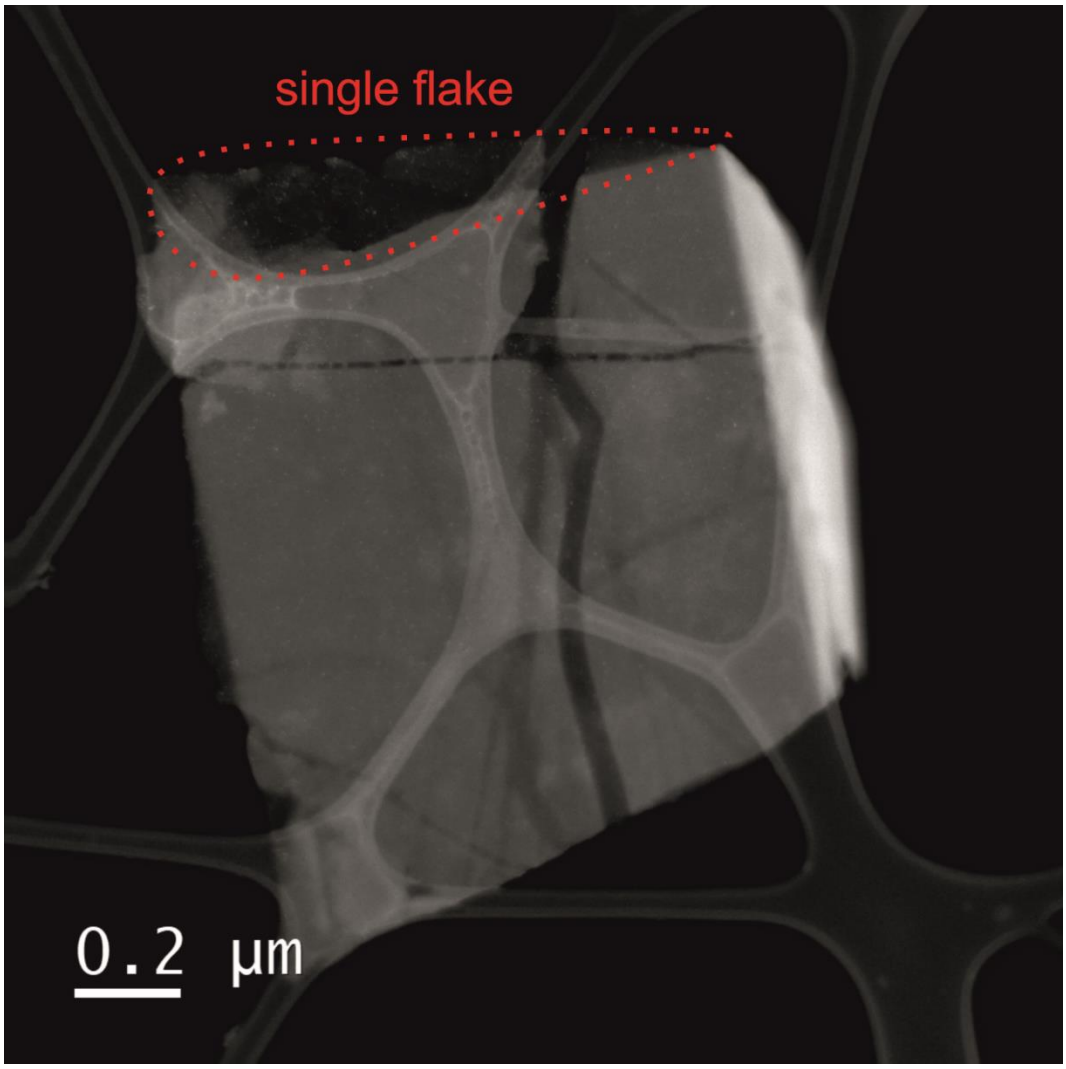

Figure S1. Low-magnification HAADF-STEM of Pd/bP on lacey carbon support film. The single flake is clearly visible by Z-contrast.

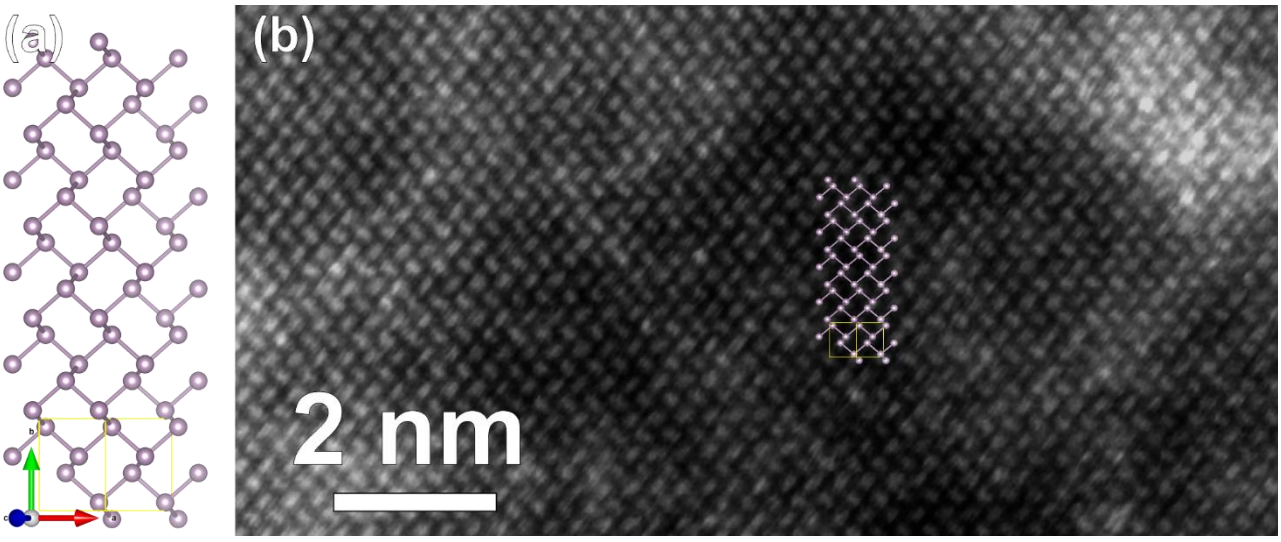

Figure S2. (a) Drawing of bP along the [101] zone axis. The yellow frame indicates the unit cell. (b) HAADF-STEM image of Pd/bP taken along the [101] zone axis. The drawing is superimposed to

emphasize the correct atomic position. Pd-rich regions can be distinguished for the higher Z-contrast (brighter areas).

1. Synthesis of Pd/ketjen black

Ketjen black (0.6 mg, 0.050 mmol) was dispersed in 1.5 mL of distilled and degassed THF by means of ultrasounds. To this black suspension, 1.3 mL of degassed ethanol were added, followed by 1.3 mL of a 3.75 mM aqueous solution of $Pd(NO_3)_2 \cdot 2H_2O$ (0.00487 mmol, Pd : C = 1:10). The mixture was transferred inside a glass vial equipped with a magnetic stirring bar. The vial was put inside an autoclave, pressurized with 5 bar of H_2 and left stirring for 1 h. After this time the autoclave was vented, the mixture was transferred in a centrifuge tube, 5.0 mL of degassed ethanol were added and the solid catalyst was isolated upon centrifugation at 9000 rpm for 30 minutes. The washing procedure was repeated two times and the final solid was dried under vacuum for 10 hours. The actual Pd content was measured by ICP-AES and resulted equal to 7.7 % mol.

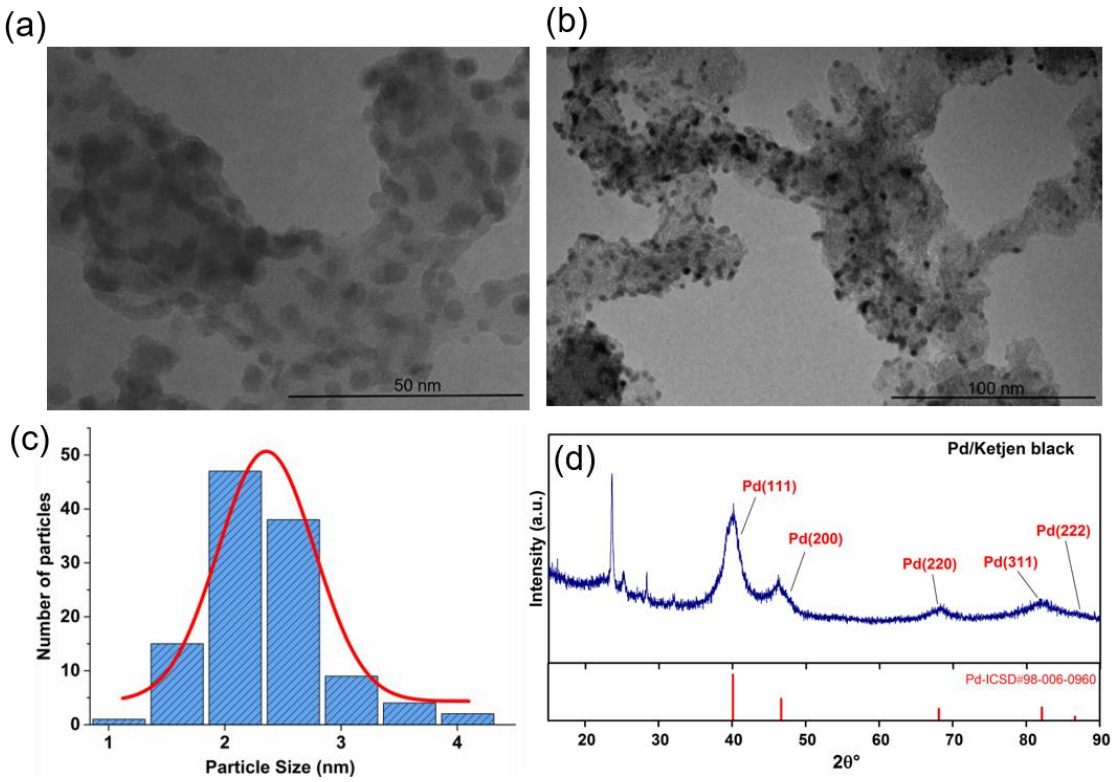

Figure S3. Characterization of Pd/ketjen black. (a) Enlarged TEM, scale bar 50 nm and (b) TEM image, scale bar 100 nm (c) Size distribution of PdNPs on ketjen black. (d) XRD pattern of Pd/ketjen black. The peak marked with an asterisk is due to an impurity from the sample holder.

2. Materials Characterization

Transmission electron microscopy. TEM studies were carried out using a Philips instrument operating at an accelerating voltage of 100 kV. Few drops of Pd/bP and Pd/ketjen black in methanol were placed on the TEM copper/carbon grid, air dried, and measured.

Scanning transmission electron microscopy. Atomic-resolution characterization by STEM was performed through a probe aberration-corrected JEOL ARM200CF, equipped with a Ceos hexapole-type Cs corrector, named CESCOR, and operated at a primary beam energy of 60 keV. The electron gun is a cold-field emission gun with an energy spread of 0.3 eV. The probe size was 1.0 Å at 60 kV. Micrographs were acquired in Z-contrast mode (High-Angle Annular Dark Field, HAADF).

A Centurio Energy Dispersive Spectrometer (EDS) equipped with a 100 mm^2 Silicon Drift Detector was used for the EDS acquisitions.

A GIF Quantum ER as Electron Energy Loss Spectrometer (EELS) was used for EELS measurements. Both low- and core-loss EELS spectra were acquired with the DualEELS capability through Gatan Digital Micrograph software, which allows the accurate energy calibration of EELS spectra, thanks to the simultaneous alignment of the zero-loss peak position for every single acquisition, which removes any artefact coming from energy shifts. The use of Fourier logarithmic deconvolution on a full spectrum obtained by splicing together low- and core-loss EELS allows removing thickness-related plural scattering.[1] All the STEM-EELS and STEM-EDS measurements were performed simultaneously by using the Gatan spectrum imaging (SI) tool.

Gas Chromatography. GC analyses were performed on a Shimadzu GC-14A gas chromatograph (with polar column) equipped with flame ionization detector and a SPB-1 Supelco fused silica capillary column (30 m, 0.25 mm i.d., 0.25 μm film thickness).

Inductively coupled plasma atomic emission spectrometer. ICP-AES measurements were performed with an Agilent 7700 Series spectrometer. Samples followed a microwave-assisted digestion in Nitric acid for trace analysis. Then, different dilutions of each sample with water for trace analysis were prepared, in order to obtain concentrations in the sensitivity range of the instrument for the elements under investigation (namely Pd and P). Standards at different concentrations have also been prepared and measured contextually to sample measurements, in order to obtain a calibration curve for each element under investigation.

Atomic force microscopy. AFM measurements were performed with a Bruker Dimension Icon Atomic Force Microscope, in pick force mode. Samples for AFM were prepared by drop cast of a suspension of Pd/bP in tetrahydrofuran/ methanol (1:1) on a Si/SiO_2 substrate. The drop was left in contact with the substrate for one minute, then the sample was washed with ethanol and dried first under a stream of nitrogen and then in vacuum for five hours. Samples prepared with this method

have almost no solvent traces, at least far from the edges, and quite small aggregates. During AFM, we approached regions where no aggregates were visible in the optical microscope, and found some thin and thick structures, the former are shown in the main text, the latter are shown in Figure S4, which are likely to be aggregates of many flakes. These structures have an average lateral dimension of 500 nm and a thickness of up to 200 nm.

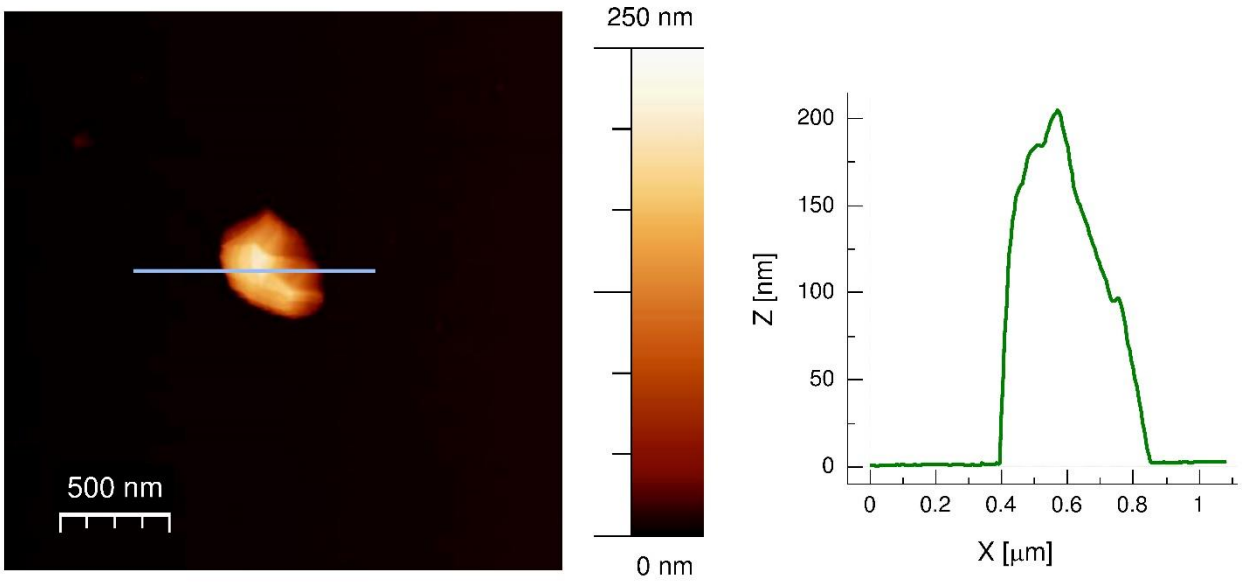

Figure S4. AFM image of Pd/bP flake.

Powder X-ray diffraction. XRD data were collected with an X'Pert PRO diffractometer operating in a Bragg-Brentano parafocusing geometry with Cu-Kα radiation (λ = 1.5418) operating at 40 kV and 30mA. Samples were prepared by slow dropcast of about 1 mg of material (Pd/bP or Pd/ketjen black) suspended in EtOH (1 mg/mL). A nitrogen flux was directed onto the sample during the dropcast to accelerate evaporation after the deposition of each drop. The process was continued until a layer of the material was uniformly distributed on the sample holder.

Raman scattering. Raman measurements were carried out using a micro-Horiba Xplora system coupled to a 532 nm wavelength laser. The backscattered light was collected by a 100× microscope objective with 0.9 NA, which generates a ~1-μm large laser beam waist. Integration times of 10 s, laser power values in the 1-2 mW range and a grating of 1200 cm^{-1} were employed. The samples were prepared by dropcasting a suspension of bP and Pd/bP in tetrahydrofuran on a Si/SiO_2 wafer. After one minute of exposure, the wafers were rinsed with ethanol and dried under a stream of nitrogen for 30 minutes. To study the influence of Pd NPs on the Raman shift of black phosphorus, Pd/bP was prepared with two different Pd loading, namely 0.5 % mol and 10% mol, using the same batch of pristine bP for both preparations. Raman spectra were collected from 15 different nanosheets in each

sample of pristine bP, Pd/bP 0.5% mol and Pd/bP 10% mol. The average Raman shift of each active mode was calculated for the three samples and is displayed in Figure S5 with relative error bars. No relevant shift in the peak positions was observed for the two Pd/bP samples compared to pristine bP.

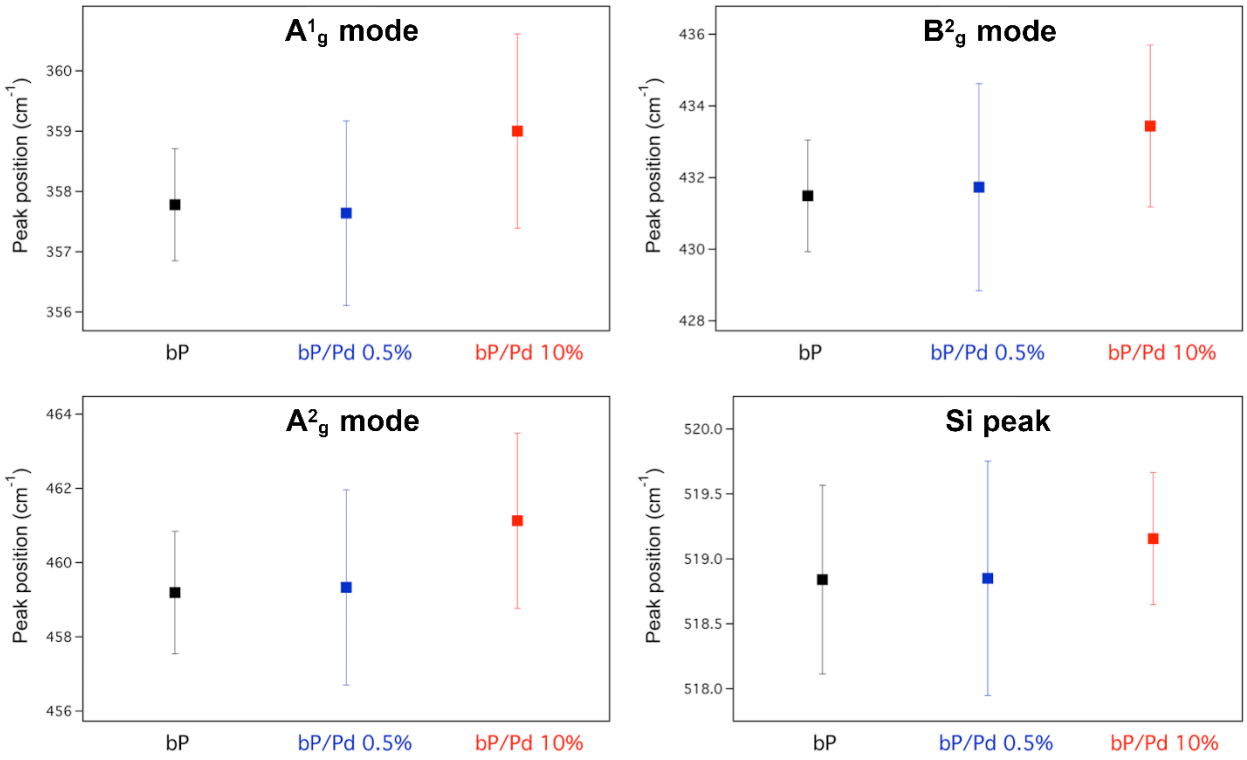

Figure S5. Comparison of Raman data of pristine bP with Pd/bP having two different loading of Pd.

Acquiring EELS spectrum at the O-K edge in the region under study, see Figure S6 below, evidenced the absence of oxygen on the surface of the nanoparticles and on bP, thus the interaction described in the main text, can only be attributed to Pd-P.

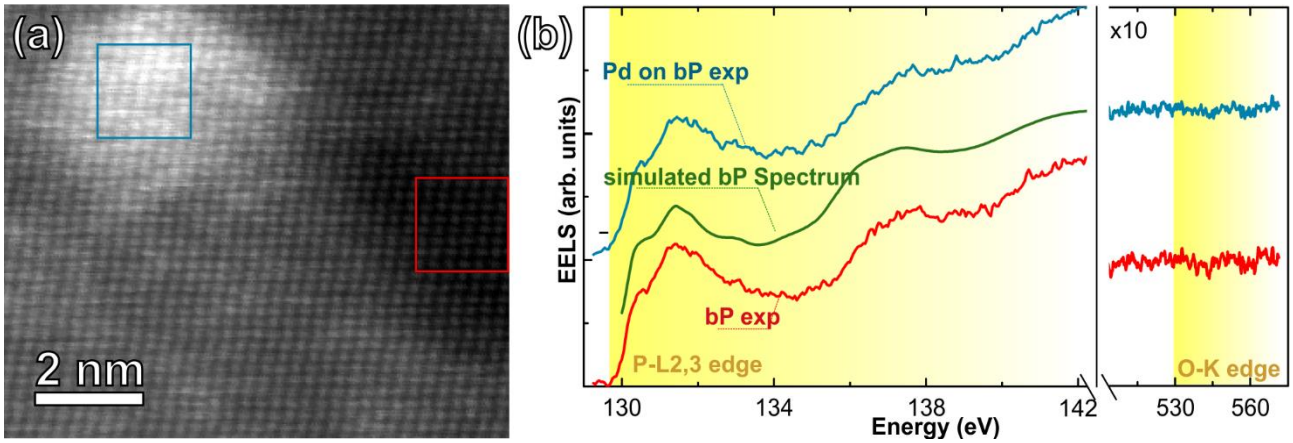

Figure S6. EELS spectra at P-$L_{2,3}$ edge and O-K edge for the sample Pd/bP.

XPS. X-ray Photoelectron Spectroscopy (XPS) measurements were performed in an ultra-high vacuum (10^{-9} mbar) system equipped with a VSW HAC 5000 hemispherical electron energy analyser and a non-monochromatized Mg-Kα X-ray source (1253.6 eV). The source power used was 100 W (10 kV×10 mA) and the spectra were acquired in the constant-pass-energy mode at E_{pas} = 44 eV. The overall energy resolution was 1.2 eV as a full-width at half maximum (FWHM) for the Ag $3d_{5/2}$ line of a pure silver reference. The recorded spectra were fitted using XPS Peak 4.1 software employing Gauss-Lorentz curves after subtraction of a Shirley-type background. The powder sample was introduced in the UHV system via a loadlock under inert gas (N_2) flux, in order to minimize the exposure to air contaminants and kept in the introduction chamber for at least 12 hours before the measurements.

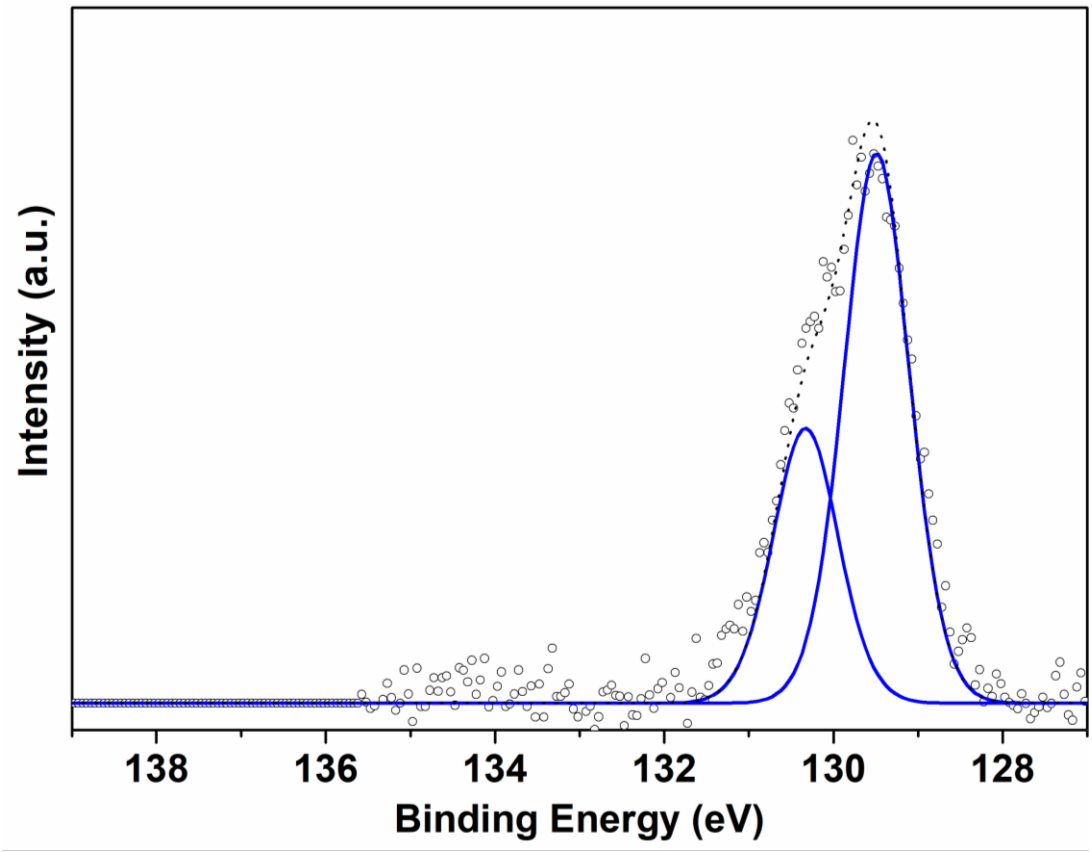

Figure S7. P 2p core level XPS spectrum of pristine bP.

X-ray Absorption Spectroscopy (XAS). To study in depth the nature of the interaction between the palladium atoms on the surface of the nanoparticles in contact with P atoms of bP sheets, X-ray Absorption Spectroscopy (XAS) experiments at the Pd-K edge (E_{edge}=24350 eV) have been carried out at the LISA beamline at the European Synchrotron Radiation Facility.[2] The monochromator was equipped with a pair of flat Si(311) crystals; collimation and harmonic rejection was achieved by

using a Pt-coated cylindrical mirror before the monochromator with an incidence angle of 2 mrad. Further harmonic rejection and focusing was achieved with a Pt toroidal mirror (focusing configuration 2:1) positioned after the monochromator. The beam size on the sample was approximately 0.2 mm. Measurements were carried out at room temperature whereas the XAS signal was collected in fluorescence mode using a 12 elements High Purity Germanium Detector. A Pd foil placed after the sample was used as energy calibration standard compound and its spectrum was always collected together with the samples. XAS data were reduced and analyzed with the ATENA/ARTEMIS codes[3,4] and the theoretical XAS signals were generated with the FEFF-8.4 code.[5] Structural parameters were obtained by data fits in R space with the transformation ranges in k space varying from case to case (k=[2.5->14] $Å^{-1}$ for for the best cases, k=[2.5->9] $Å^{-1}$ for the noisier spectra) and a k^2 weight factor. Coordination Numbers (CNs) have been calibrated via the analysis of the Pd metal foil, finding a global amplitude correction factor S_0^2=0.88.

EXAFS analysis EXAFS (extended X-ray absorption fine structure) analysis was carried out modeling the data with two contributions: Pd clusters and Pd-P bond. The model of Pd clusters included 4 coordination shells for Pd foil though in Table S2 only the first shell is presented. The others were modelized with a single Pd-Pd first shell, other coordination shells being not visible in the FT. An additional Pd-P bond was added to account for the interaction with phosphorus atoms as evidenced by the peak in the FT below 2 Å. For comparison the spectrum of a PdO sample has been analysed with a model consisting in two shells: PdO and Pd-Pd. The last three rows of Table S2 show the crystallographic data for different model compounds.

Table S1. Description of the samples studied by XAS

Sample	Description
Pd/bP	Pd NPs on bP nanosheets (aver. size 3.1±0.8nm)
Pd@PTA	PTA-capped Pd NPs (aver. size 3.2 ± 0.4nm)
PdP_2	PdP_2 NPs
Pd/C	Pd NPs on carbon (aver. size 2.0 ± 0.4nm)
Pd foil	Pd metal foil at RT
PdO	PdO powder at RT

Table S2. Results of the quantitative XAS analysis. CNs $_{PdX}$ = average coordination number with atom 'X', R_{PdX} (Å) = Pd-X distance; σ^2_{PdX} (Å^2) Debye-Waller factor of the PdX bond. Errors on the last digit are given in brackets. The numbers in apex, 6, 7, 8, 9, 10 refer to literature references.

Sample	CNs Pd-O *Pd-C*	R_{PdO}(Å)	σ^2_{PdO} (Å^2)	CNs Pd-P	R_{PdP}(Å)	σ^2_{PdP} (Å^2)	CNs Pd-Pd	R_{PdPd}(Å)	σ^2_{PdPd} (Å^2)
Experimental values									
Pd metal							12	2.74(1)	0.0059(4)
Pd/C	*4(2) C*	*1.94(3)*	*0.013(5)*				7(2)	2.73(1)	0.0065(5)
Pd/bP				1.7(6)	2.26(3)	0.0018(6)	8(2)	2.77(3)	0.016(4)
Pd@PTA[6]				0.7(2)	2.25(3)	0.004	8(2)	2.73(2)	0.009(2)
PdP_2				3.8(6)	2.32(2)	0.004(2)			
PdO	4	2.01(2)	0.002(1)				4 8	3.04(3) 3.43(3)	0.0038(6)
Literature values									
PdP_2[7]				2 2	2.335 2.341	-			
PdP_3[8]				6	2.235	-			
Pd metal[9]							12	2.7453	-
PdO[10]	4	2.018	-				4 8	3.030 3.419	-

3. Catalytic hydrogenation of nitroarenes and recycling tests.

In a typical run, 1-chloro-2-nitrobenzene (114.2 mg, 0.725 mmol) was added to the solid catalyst Pd/bP 10% mol (1.3 mg bP, 0.042 mmol, 0.044 mmol Pd) in a screw capped centrifuge tube, 3 mL of degassed MeOH were added and the mixture was sonicated for 5 minutes to suspend the catalyst and dissolve the substrate. The suspension was then transferred in a glass vial placed inside an autoclave and equipped with a magnetic stirring bar. The autoclave was purged with hydrogen (3 times) and then pressurized up to 5 bar. The mixture was kept stirring for the required time, after which the gas was vented and the mixture was transferred in a centrifuge tube. 5 mL of degassed MeOH were added and the suspension was centrifuged at 9000 RPM for 30 minutes. The supernatant was analysed by GC. To the solid residue containing the catalyst, the nitroarene and methanol were added, and a new catalytic run was launched.

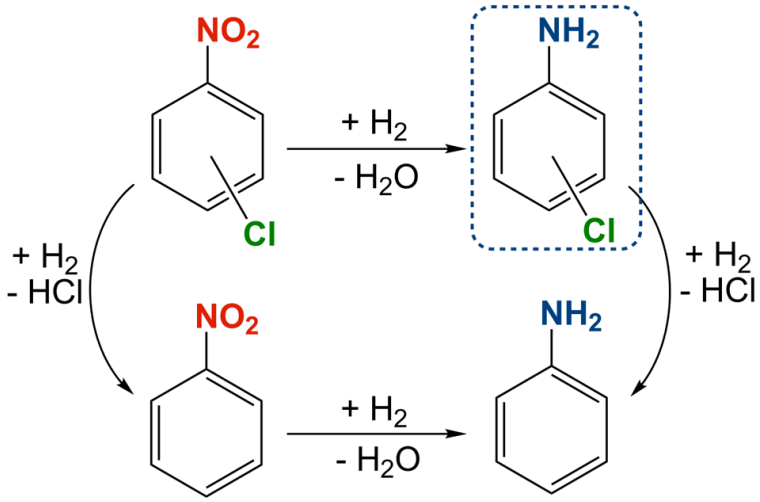

Figure S8. The two possible pathways for the secondary reaction of C-Cl hydrogenolysis.

Table S3. Catalytic tests on the reduction of nitroarenes.

Catalyst	Substrate	Time (min)	Sub/cat	Conversion%[a]	Selectivity%[b]	TOF[c] (h^{-1})
Pd/bP	1-chloro-3-nitrobenzene	30	162	99.1	97.7	313
	1-chloro-2-nitrobenzene	40	162	99.5	97.3	235
Pd/C	1-chloro-2-nitrobenzene	30	191	99.9	78.1	298

Reaction conditions: solvent: methanol, [substrates] = 0.242 M; room temperature; 5 bar H_2; magnetic stirring, 1200 rpm. Sub/Cat: substrate/catalyst ratio (mol/mol). [a]Data from GC analysis and GC-MS; [b] the remaining is aniline; [c] Turn over frequency.

4. Test for the heterogeneous nature of the catalyst, ruling out the presence of catalytically active species in solution.

A catalytic run was started under the standard reaction conditions described above. After 15 minutes the reaction was stopped, the autoclave was vented and the reaction mixture was transferred in a centrifuge tube. The solid material was isolated by centrifugation at 9000 RPM for 30 minutes. A small fraction of the supernatant (2 µL) was taken for GC-MS analysis, Entry 1 in Table S3. The remaining was transferred in the autoclave, pressurized with 5 bar of H_2 and kept stirring for 40 minutes. After this time the autoclave was vented and GC-MS analysis was carried out. The supernatant gave no further conversion (Entry 2), confirming that the catalytic activity is due entirely to the solid phase.

A further catalytic run was performed recycling the recovered solid catalyst under the same reaction conditions. Results comparable with fresh catalyst Pd/bP were obtained, see Entry 3.

Table S4.

Entry	Catalytic run	Time (min)	Conversion%	Selectivity%	TOF (h^{-1})
1	1st run, Pd/bP	15	42.6	95.1	263
2	no solid phase	40	42.8	94.7	-
3	1st recycle, Pd/bP	40	97.8	90.7	215

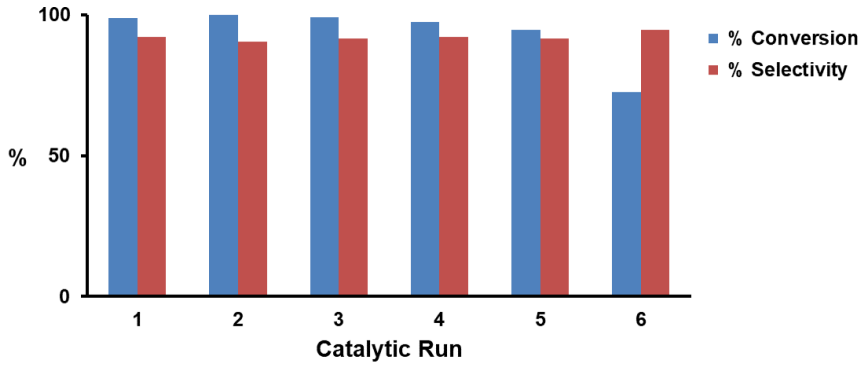

Figure S9. Catalyst reuse in the hydrogenation of 1-chloro-2-nitrobenzene.

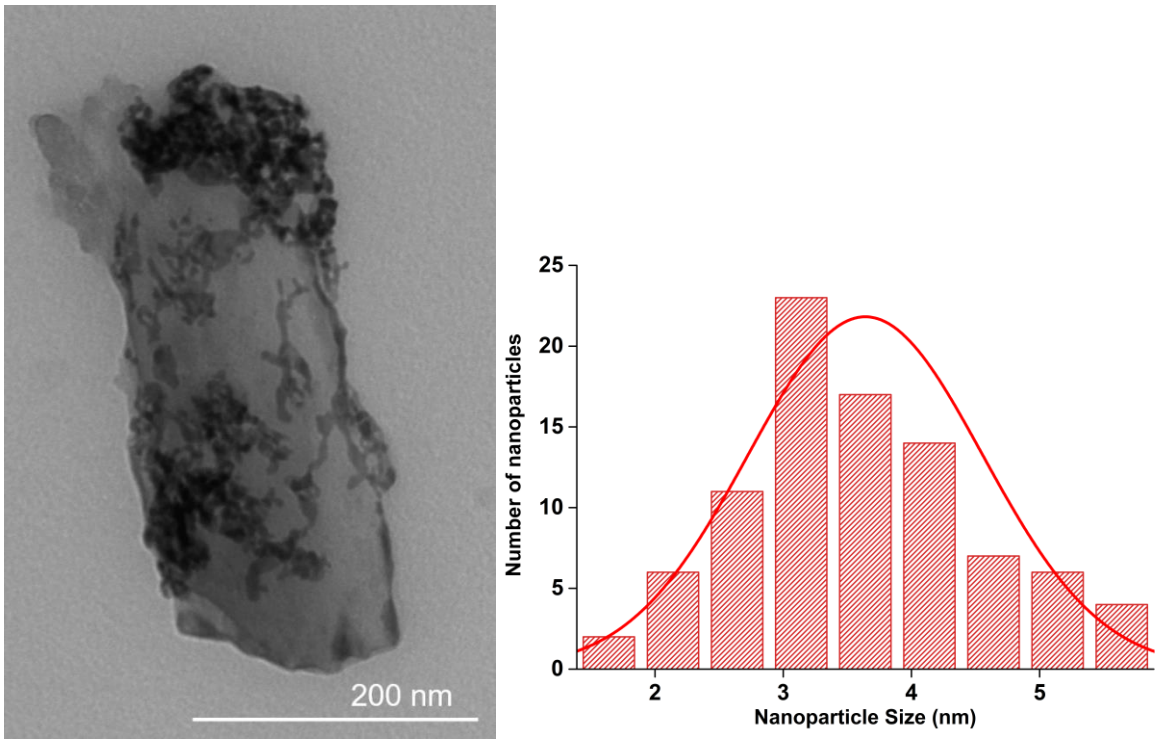

Figure S10. TEM image of Pd/bP after catalytic tests and relative size distribution of the palladium nanoparticles.

References

(1) Scott, J.; Thomas, P. J.; MacKenzie, M.; McFadzean, S.; Wilbrink, J.; Craven, A. J.; Nicholson, W. A. P. Near-simultaneous dual energy range EELS spectrum imaging. *Ultramicroscopy* **2008**, *108*, 1586.

(2) D'Acapito, F.; Lepore, G. O.; Puri, A.; Laloni, A.; la Manna, F.; Dettona, E.; de Luisa. A.; Martin, A. The LISA beamline at ESRF. *J. Synchrotron Radiat*. **2019**, *26*, 551.

(3) Newville, M. *IFEFFIT*: interactive XAFS analysis and *FEFF* fitting. *J. Synchrotron Rad*. **2001**, *8* 322.

(4) Ravel, B.; Newville, M. *ATHENA, ARTEMIS, HEPHAESTUS*: data analysis for X-ray absorption spectroscopy using *IFEFFIT*. *J. Synchrotron Rad*. **2005**, *12*, 537–41.

(5) Ankudinov, A. L.; Ravel, B.; Rehr, J. J.; Conradson, S. D. Real-space multiple-scattering calculation and interpretation of x-ray-absorption near-edge structure. *Phys. Rev. B* **1998**, *58*, 7565.

(6) Caporali, M.; Guerriero, A.; Ienco, A.; Caporali, S.; Peruzzini, M.; Gonsalvi, L. Water-Soluble, 1,3,5-Triaza-7-Phosphaadamantane-Stabilized Palladium Nanoparticles and their Application in Biphasic Catalytic Hydrogenations at Room Temperature. *Chem. Cat. Chem*. **2013**, *5*, 2517 – 2526.

(7) Zachariasen, W. H. The Crystal Structure of Palladium Diphosphide. *Acta Cryst*. **1963**, *16*, 1253.

(8) Rundqvist, S. Phosphides of the Platinum Metals. *Nature* **1960,** *185*, 31.

(9) Owen, E. A.; Yates, E. L. Precision measurements of crystal parameters. *Philosophical Magazine*, **1933**, *15*, 472.

(10) Waser, J.; Levy, H. A.; Peterson, S. W. The structure of PdO. *Acta Cryst*. **1953**, *6*, 661.